Stabilization of Gaze during Early Xenopus Development by Swimming-Related Utricular Signals.

François Lambert, Julien Bacqué-Cazenave, Anne Le Seach, Jessica Arama, Gilles Courtand, Michele Tagliabue, Selim Eskiizmirliler, Hans Straka, Mathieu Beraneck

Current Biology Swim style-dependent utricular activation ensures gaze-stabilization during early development –Manuscript Draft– Manuscript Number: CURRENT-BIOLOGY-D-19-01330R2 Full Title: Swim style-dependent utricular activation ensures gaze-stabilization during early development Article Type: Report Corresponding Author: Powered by Editorial Manager® and ProduXion Manager® from Aries Systems Corporation

François Lambert, Julien Bacqué-Cazenave, Anne Le Seach, Jessica Arama, Gilles Courtand, Michele Tagliabue, Selim Eskiizmirliler, Hans Straka, Mathieu Beraneck

Current Biology

Swim style-dependent utricular activation ensures gaze-stabilization during early development

--Manuscript Draft--

Manuscript Number:	CURRENT-BIOLOGY-D-19-01330R2
Full Title:	Swim style-dependent utricular activation ensures gaze-stabilization during early development
Article Type:	Report
Corresponding Author:	Francois Michel Lambert, PhD Centre National de la Recherche Scientifique Bordeaux, FRANCE
First Author:	Francois M Lambert, PhD
Order of Authors:	Francois M Lambert, PhD
	Julien Bacque-Cazenave
	Anne Le Seach
	Jessica Arama
	Gilles Courtand
	Michele Tagliabue
	Selim Eskiizmirliler
	Hans Straka
	Mathieu Beraneck
Abstract:	Locomotor maturation requires concurrent gaze stabilization improvement for maintaining visual acuity [1, 2]. The capacity to stabilize gaze, in particular in small aquatic vertebrates where coordinated locomotor activity appears very early, is determined by assembly and functional maturation of inner ear structures and associated sensory-motor circuitries [3-7]. Whereas utriculo-ocular reflexes become functional immediately after hatching [8, 9], semicircular canal-dependent vestibulo-ocular reflexes (VOR) appear later [10]. Thus, small semicircular canals are unable to detect swimming-related head oscillations, despite the fact that corresponding acceleration components are well-suited to trigger an angular VOR [11]. This leaves the utricle as sole vestibular origin for swimming-related compensatory eye movements [12, 13]. We report a remarkable ontogenetic plasticity of swimming-related head kinematics and vestibular endorgan recruitment in Xenopus tadpoles with beneficial consequences for gaze-stabilization. Swimming of older larvae generates sinusoidal head undulations with small, similar curvature angles on the left and right side that optimally activate horizontal semicircular canals. Young larvae swimming causes left-right head undulations with narrow curvatures and strong, bilaterally dissimilar centripetal acceleration components well-suited to activate utricular hair cells and to substitute the absent semicircular canal function at this stage. The capacity of utricular signals to supplant semicircular canal function was confirmed by recordings of eye movements and extraocular motoneurons during off-center rotations in control and semicircular canal-deficient tadpoles. Strong alternating curvature angles and thus linear acceleration profiles during swimming in young larvae therefore represents a technically elegant solution to compensate for the incapacity of small semicircular canals to detect angular acceleration components.

Swim style-dependent utricular activation ensures gaze-stabilization during early development

Francois M. Lambert[1*#], Julien Bacqué-Cazenave[1*], Anne Le Seach[2], Jessica Arama[2], Gilles Courtand[1], Michele Tagliabue[2], Selim Eskiizmirliler[2], Hans Straka[3,*], Mathieu Beraneck[2,*#]

[1] INCIA, CNRS UMR 5287, Université de Bordeaux, F- 33076 Bordeaux, France

[2] Université de Paris, Integrative Neuroscience and Cognition Center, CNRS UMR 8002, F-75270 Paris, France.

[3] Department Biology II, Ludwig-Maximilians-University Munich, Grosshadernerstr. 2, 82152 Planegg, Germany

* FM.L. and J.B. contributed equally to this work.

* H.S. and M.B. contributed equally to this work.

Key words: Swimming, kinematics, vestibular system, otolith organ, semicircular canal, vestibulo-ocular reflex

Running title: Head motion kinematics and eye movement during swimming

Correspondence:

Dr. François M. Lambert (Lead Contact). Institut de Neurosciences Cognitives et Intégratives d'Aquitaine, CNRS UMR 5287, Université de Bordeaux, France. Email: francois.lambert@u-bordeaux.fr

Dr. M. Beraneck. Integrative Neuroscience and Cognition Center, CNRS UMR 8002, Université de Paris, 45 rue des St-Pères, Paris 75270, France. Email: mathieu.beraneck@parisdescartes.fr

SUMMARY

Locomotor maturation requires concurrent gaze stabilization improvement for maintaining visual acuity [1, 2]. The capacity to stabilize gaze, in particular in small aquatic vertebrates where coordinated locomotor activity appears very early, is determined by assembly and functional maturation of inner ear structures and associated sensory-motor circuitries [3-7]. Whereas utriculo-ocular reflexes become functional immediately after hatching [8, 9], semicircular canal-dependent vestibulo-ocular reflexes (VOR) appear later [10]. Thus, small semicircular canals are unable to detect swimming-related head oscillations, despite the fact that corresponding acceleration components are well-suited to trigger an angular VOR [11]. This leaves the utricle as sole vestibular origin for swimming-related compensatory eye movements [12, 13]. We report a remarkable ontogenetic plasticity of swimming-related head kinematics and vestibular endorgan recruitment in *Xenopus* tadpoles with beneficial consequences for gaze-stabilization. Swimming of older larvae generates sinusoidal head undulations with small, similar curvature angles on the left and right side that optimally activate horizontal semicircular canals. Young larvae swimming causes left-right head undulations with narrow curvatures and strong, bilaterally dissimilar centripetal acceleration components well-suited to activate utricular hair cells and to substitute the absent semicircular canal function at this stage. The capacity of utricular signals to supplant semicircular canal function was confirmed by recordings of eye movements and extraocular motoneurons during off-center rotations in control and semicircular canal-deficient tadpoles. Strong alternating curvature angles and thus linear acceleration profiles during swimming in young larvae therefore represents a technically elegant solution to compensate for the incapacity of small semicircular canals to detect angular acceleration components.

RESULTS

Eye motion dynamics during free-swimming

The ability of *Xenopus* tadpoles to stabilize gaze during free swimming was evaluated from high-frequency video recordings at two larval stages (stage 47, n = 7; stage 57, n = 5; Figure 1A1,2). Reconstruction of eye-in-space and head-in-space trajectories over several consecutive swim cycles (Figure 1B1,2) revealed

that animals at both developmental stages produce conjugate eye movements in phase-opposition to head movements (Figure 1C1,2) with comparable ranges of ocular excursion angles (5-30°) and degrees of eye-head correlation (Figure 1D). Eye motion magnitudes were maximal (eye-in-head ratio ~1) for small head oscillations (<10°) and minimal (~0.3) for large head oscillations (>40°; Figure 1E), indicating that gaze stabilization is equally effective at both stages and thus independent of larval size or morphometric characteristics. Because tadpoles at the two stages differ in their capacity to encode angular head acceleration [10], potential ontogenetic changes of head motion kinematics were evaluated.

Swim speed and head oscillation kinematics

Kinematic parameters were obtained from a total of 125 swimming episodes (n = 65 for stage 47; n = 60 for stage 57; 16 animals each). Even though the swim speed of individual animals was rather variable (Figure 1F), older larvae generally swam faster than younger larvae (Figure 1G; $p < 0.001$ Mann-Whitney U-test). While the distribution of swim speeds overlapped in the low velocity range, stage 57 tadpoles reached considerably higher velocities compared to stage 47 larvae (Figure 1H) with smaller variance as indicated after normalization to the average speed (Figure 1I).

The capacity to effectively stabilize gaze was estimated by reconstructing head trajectories during swimming (green and blue lines in Figure 2A,B) from the highly contrasted outline of the eyeball on each side. While tadpoles at both stages produced left-right head movements during swimming, stage 47 larvae exhibited strong, alternating excursions of the head to both sides (Figure 2A1-3). During each swim cycle, the eyeball on the inner side of the head turn remained almost stationary in space (green inward marks in Figure 2A2-3). The minimal displacement for ~60 ms (Figure 2C, black trace) corresponded to the low velocity on the side of the inward curve (2.6 ±1.6 cm/s; Figures 2D, S2E). Simultaneously, the outer side of the head turn (blue outward marks in Figure 2A2-3) advanced considerably farther forward. During the second half cycle, this forward progression profile was inverted (Figure S2E).

At stage 57, the head exhibited a more rectilinear motion pattern (Figure 2B1-3). During maximal head excursion, the eyeball on the inner side of the head turn moved rather constantly (Figure 2C, red trace) and with a considerably faster velocity (6.4 ±2.9 cm/s; mean eye velocity $p < 0.001$ Mann-Whitney U-test; Figure 2D, S2E) compared to young larvae. Velocities at normalized swimming speed (Figure 2E) confirmed that the inner side of the head turn experienced a longer stationary phase at stage 47 than at stage 57 and thus requires dynamically different compensatory eye movements, which might derive from different sets of vestibular endorgans.

Stage-dependent swim motion-related acceleration components

Effective head motion parameters during swimming, as relevant stimulus for vestibular endorgans, were calculated from the triangulated trajectories of the inner ears (otic capsule, OC in Figures S1A,D,E; Figure 2A,B). The head of stage 47 larvae rotates around alternating eccentric vertical axes located only at a distance of 1-5 mm from the center of the eyeball. This causes the ear on the inner side to follow a narrow curve and on the outer side to proceed along a wider path (Figure 2A3). Ears of stage 57 tadpoles follow trajectories around rather distant rotation axes (>5 mm) with comparably wide curvature angles (Figure 2B3). During each head turn, the maximum curvature of the ear on the inner and outer side is thus highly different on the left and right side of the head for each half-cycle at stage 47, but bilaterally more similar at stage 57 (black and red traces in Figure 2F,I). This was confirmed after cycle-by-cycle averaging and quantification of the motion trajectory of both ears (Figure 2G,H,I; mean maximal curvature, $p < 0.001$ in H and $p<0.0001$ in I, Mann-Whitney U-test).

The magnitudes of angular acceleration and forward, lateral and centripetal linear acceleration at peak curvature were calculated separately during each swim cycle at the level of the vestibular endorgans (OC; Figures S1E, S3). The more pronounced peak curvature at stage 47 causes considerably larger centripetal linear accelerations (Figure 2J, S3A4) compared to stage 57, whereas forward, lateral and angular accelerations were stage-independent (Figure S3B1-3). Thus, swimming in young tadpoles causes pronounced left/right dissimilar translational acceleration components whereas older larvae experience only small, left-right similar centripetal acceleration components.

Otolith-ocular eye movements as substitute for deficient semicircular canal-ocular reflexes

Eye movements were recorded in head-fixed semi-intact preparations (stage 47, n = 7) in the absence of visual and proprioceptive sensory signals and spinal locomotor efference copies. In stage 47 tadpoles, semicircular canal-evoked eye movements during sinusoidal head-center rotations (1 Hz and ±120°/s) were absent (Figure 3A1) as previously reported [10]. In contrast, robust conjugate utricle-derived eye oscillations were recorded during cyclic lateral head translations, Figure 3A2). To evaluate a utricular contribution to gaze-stabilization during swimming, stage 47 tadpole preparations were rotated around eccentric vertical rotation

axes, located 5 mm outside the head, respectively. Such off-center head rotations produced conjugate eye movements with a gain of ~0.2 during both left-out (Figures 3A3) and right-out rotations (Figures S4B). Despite relatively small gains, eye movements were robust, directionally appropriate and likely derived from an asymmetric activation of bilateral utricular hair cells corroborating previous results in adult frogs [14]. Recordings of lateral rectus (LR) nerve activity during rotation around different axes (1 Hz; ±30-240°/s) as more precise functional output confirmed a differential horizontal semicircular canals and utricular activation (Figure S4F). The larger discharge modulation during rotation around an eccentric *versus* centered axis (Figure S4F2,3) likely derives from utricular signals, supporting the conclusions drawn from eye motion recordings.

A predominant if not exclusive utricular origin of swim-related compensatory eye movements was substantiated by two further sets of experiments. First, bilateral injections of 0.5% MS-222 into the otic capsule, known to block vestibular afferent spike discharge [15] reversibly abolished both translational and eccentric rotational motion-evoked eye movements (Figures 3A2,3 red traces, S4C). Second, bilateral semicircular canal-deficient stage 50 larvae were generated by hyaluronidase injections into both otic capsules at stage 44, as previously described in *Xenopus* [16-18]. As confirmation for the absence of bilateral semicircular canals and in compliance with prior studies [17, 18], these animals completely lacked cyclic eye movements during rotation around a centered vertical axis (Figure 3B1,C1). However, lateral translation (Figure 3B2,C2) as well as rotation around eccentric axes (Figures 3B3,C3, S4E) evoked robust, compensatory eye movement. In the absence of all other motion-related sensory signals, these experiments therefore collectively confirm a utricular origin of these eye movements and suggest that the swim style of young tadpoles is able to recruit otolith-ocular pathways for gaze-stabilization.

DISCUSSION

Swimming of stage 47 in contrast to stage 57 larvae is accompanied by strongly curved head trajectories that bilaterally alternate during each swim cycle (Figure 4). The pronounced curvature profile causes considerable centripetal acceleration components and differentially activates utricular signals on both sides that dominate reactive compensatory eye movements, supplanting the negligible angular VOR of young tadpoles.

Developmental plasticity of swimming performance

Tadpoles between stage 47 and 57 experience a 3-4 fold increase in body length, whereas the morphometric ratio of several anatomical markers (Figure S1B) and normalized swim speed remain constant. While this suggests similar swimming dynamics and scaling of forward thrust magnitude with increasing tail propulsive capacity, forward motion is achieved by different propulsive dynamics, respectively (Figures 4A). Parameters such as tail thickness and elastic capacity, relevant for tail bending, are non-linearly scaled with body growth [11]. Thus, the relatively larger mass of the head/body with respect to the tail [19] and smaller Reynolds numbers of small larvae [20] are obviously more relevant factors for stage-specific swim style dynamics. Independent of head motion kinematics, however, gaze-stabilizing eye movements are generated throughout development.

Role of predictive signals for gaze-stabilizing eye movements

The occurrence of predictable visual perturbations during rhythmic locomotor activity, allows gaze-stabilizing eye movements to be evoked by intrinsic copies of the propulsive motor commands [21, 22]. Spinal locomotor efference copies in larval *Xenopus* initiate compensatory eye movements during swimming [11, 23]. While initially demonstrated for mid-larval stages, spino-extraocular motor coupling could also play an important role for gaze-stabilization in young larvae. Compensatory eye movements appear early in development, along with free swimming [24] and the maturation of the underlying spinal network [25]. Despite the peculiar motion trajectory, the stereotypic swim style of young larvae make locomotor efference copies nonetheless suitable to elicit gaze-stabilizing eye movements. This feedforward connectivity is however calibrated by vestibular sensory feedback [11,24], which during ontogeny shifts in correspondence with the swim style-related head motion kinematics from utricular only- to utricular and semicircular canal-based signals.

Role of vestibular signals for gaze-stabilizing eye movements

Gaze-stabilizing eye movements derive from a co-joint activation of semicircular canal and otolith organs [14]. Following vectoral decomposition of angular and linear head/body motion components by the endorgans, signals with common spatial field sensitivity converge at the level of central vestibular neurons [26-28]. In compliance with such a fusion, the lateral utricular epithelial sector activates lateral rectus and synergistic medial rectus motoneurons in rats [29] and frogs [30] during left-right translational motion to produce conjugate horizontal eye movements comparable to those during yaw-axis head rotation [14]. This

extraocular motor pattern is ideally suited to compensate the presumed horizontal image shifts during such head movements and is likely present in all vertebrates [31]. This varies from the general notion that activation of the lateral utricular sector should elicit vertical/oblique eye movements during roll motion [6, 8], and is potentially related to the neuronal computation underlying a disambiguation of tilt and translational motion. The pronounced central convergence of signals from the horizontal semicircular canal and a lateral utricular epithelial sector [26] thus indicates that different VOR components are not transmitted separately but rather share a common pathway. Within this circuitry, the respective acceleration components are transformed into a single spatio-temporally specific extraocular motor output. Thus, compensatory eye movements during head/body motion originate from sensory-motor processing of co-jointly activated angular and linear head acceleration vectors [14].

During ontogeny, the angular and linear VOR become functional with different time courses that depend on the establishment of the neuronal circuitry, computational capacity of individual cellular elements and physical integrity of the sense organs [1, 3, 5, 7]. In compliance with the simpler structure of otolith organs [33], graviceptive gaze-stabilizing and postural reflexes appear very early during ontogeny [1, 12, 13, 32]. In contrast, the functionality of the angular VOR depends on sufficiently large semicircular canals to allow endolymph flow during head rotation [34-37], which is particularly critical for small vertebrates such as fish or amphibian larvae [9, 10]. This limitation causes the horizontal angular VOR in *Xenopus* tadpoles to become functional only at stage 49 [10], precluding semicircular canal signals as the origin of gaze-stabilizing eye movements prior to this stage.

The absence of a functional angular VOR in young *Xenopus* larvae could be however supplanted by a functionally equivalent, otolith-derived VOR, provided that the head motion contains the relevant sensory (i.e. linear acceleration) stimuli. This assumption is supported by the finding that angular acceleration in the mammalian vestibular system can be encoded by a linear accelerometer [38,39]. This complies with our finding that adequate compensatory eye movements are activated in semicircular canal-deficient tadpoles (Figure 3B,C). In the absence of semicircular canals, the eye movement-eliciting sensory signals must derive from the utricle(s). Accordingly, activation of utricular signals by bilaterally alternating centripetal, linear acceleration components can evoke spatially specific compensatory eye movements that contribute to offsetting the visual perturbations of swimming-related head motion. The generation of linear acceleration signals during swimming in young *Xenopus* larvae therefore represents a technically elegant solution to overcome the incapacity of small semicircular canals to detect angular acceleration components and to drive an angular VOR.

Acknowledgments

The authors thank M. Patrice Jegouzo and Philippe Chauvet for their technical help in designing the experiments, and Bruno Della-Gaspera and Lionel Para-Iglesias for their help with tadpole husbandry. The authors thank the Computer-Integrated Systems for Microscopy and Manipulation at the University of North Carolina at Chapel Hill for making the video Spot Tracker version 05.23 available; credit for this software: CISMM at UNC-CH, supported by the NIH NIBIB (NIH 5-P41-RR02170). This work was supported by the ANR Grant ANR-08-BLAN-0145-01 and ANR-15-CE32-0007-02 and by the German Science Foundation (STR478/3-1). MB & MT received support from the Centre National des Etudes Spatiales. FML received support from the INCIA CNRS UMR5287.

Author Contributions

Conceptualization: FML; HS; MB;

Methodology: FML; JBC; ALS; JA; GC; MT; SE; HS; MB

Software: ALS; GC; MT; SE

Formal analysis: FML; JBC; ALS; JA; GC; SE; MB

Investigation: FML; JBC; ALS; JA; MB

Writing original manuscript: FML; SE; HS; MB

Writing – review and editing: FML; JBC; MT; HS; MB

Visualization: FML; JBC; JA; SE; HS; MB

Supervision: FML; HS; MB

Project administration: FML; MB

Funding acquisition: FML; HS; MB

Declaration of Interests

The authors declare no competing interests.

FIGURE LEGENDS

Figure 1. Compensatory eye movements during free swimming.

(A) Frame-by-frame motion trajectory of larval swimming at stage 47 (A1) and 57 (A2) obtained from high-speed videos.

(B and C) Representative examples of multiple cycles (B) and average (±SD, shaded area) over a single cycle (C) of swimming-related head and concurrent compensatory movements of the left (Le) and right (Ri) eye at stage 47 (B1 and C1) and 57 (B2 and C2).

(D and E) Scatter plots of eye excursion angle (D) and eye in head ratio (excursion angles of eye/head, E) as function of the head excursion angle.

(F and G) Mean swim speed as function of body length (F) at stage 47 (n = 25) and stage 57 (n = 27) and distribution of mean swim speeds (G); *** $p < 0.001$ (Mann-Whitney U-test).

(H and I) Distribution of absolute (H) and normalized average swim speed (I; relative to average swim speed, see G).

Figure 2. Comparison of head motion trajectories.

(A and B) Head trajectory (A1 and B1, see videos S1 and S2); magnified views of the head turn (A2 and B2) over a period of 60 ms (dashed rectangular area marked with * in A1 and B1) during swimming of stage 47 (A) and 57 (B) tadpoles; note that the displacement of the inner side of the head turn (green) causes the head movements (interconnecting lines between the eyes in A2 and B2) to be more accentuated in younger animals; frame-by-frame position of eyeballs and inner ears at the peak of the head turn (A3 and B3) indicate the curvature and the direction (dashed lines) on the inner ear from the first to the last image of the 60 ms time window;

(C) Trajectory (mean ±SEM) of the inner side of the head turn, averaged over 60 ms at the peak of the rotation (A2 and B2) during the swimming episode shown in A1 and B1.

(D) Mean velocity of the eye on the inner side of the head turn; note the overall smaller velocity in stage 47 animals; *** $p < 0.001$ (Mann-Whitney U-test).

(E) Scatter plot depicting the velocity of the inner side of the head turn as a function of normalized swimming speed.

(F) Trajectory of the inner ear (otic capsule, OC) on the inner (dark red, black) and outer side (light red, gray) of the head turn over several swim cycles; note the difference in curvature magnitudes at the two stages and the complete overlap of the trajectories of the inner and outer side (red) at stage 57.

(G-I) Trajectory (mean ±SEM) of the inner ear on the inner (dark) and outer side (light) of the head turn (G) averaged from the cyclic swim-related head motion shown in A1 and B1and F; mean ±SD of the maximal (H) and Delta curvature (left - right inner ear curvature, I) obtained from all sequences; note that the trajectories of the inner and outer side overlap completely at stage 57 (G); *** $p < 0.001$, **** $p < 0.0001$ (Mann-Whitney U-test).

(J) Distribution of centripetal linear acceleration at the level of the inner ears during swimming; corresponding distributions of forward, lateral and angular accelerations are illustrated in Figure S3; **** $p < 0.0001$ (Kolmogorov-Smirnov test).

Figure 3. Influence of rotation axis position on eye movements in tadpoles with intact, pharmacologically impaired or semicircular canal-deficient inner ears.

(A) Movement of the left (dark traces) and right (light traces) eye at stage 47 during horizontal rotation with the vertical axis in the center (A1, blue), left-right linear translation (A2, pink; see videos S3) and during off-center (A3; Le-out, purple; see videos S4) under control condition (blue traces) and after injection of 0.5% MS-222 into both inner ears (red traces); note that the robust conjugate compensatory eye movements during translation (A2) and off-center rotation (A3) were completely abolished by the local anesthetic.

(B and C) Four successive motion cycles (B) and average over a single cycle (mean ±SEM, C) of the left (dark traces) and right eye (light traces) during horizontal rotation with the vertical axis in the center (B1 and C1, blue), left-right linear translation (B2 and C2, pink) and during off-center (B3 and C3; Le-out, purple) in a semicircular canal-deficient stage 50 tadpole (n = 5); note the absence of eye movements during centered vertical-axis rotations and their persistence during off-center rotations and translations.

Figure 4. Developmental plasticity of locomotor dynamics and corresponding inner ear organ recruitment.

(A) Presumed differential activation of the utricle (utr.), semicircular canals (can.) VOR and spinal feedforward efference copies (Sp. ffwd) during swimming at stage 47 and 57 (upper row) in correspondence with changes of head centripetal acceleration and curvature profiles (lower rows).

(B) Swim pattern and spatial displacement of the bilateral utricle during the different swimming-related head rotations at stage 47 (left) and stage 57 (right) between time point *tn-1* (gray) and time point *tn* (black); linear, utricular (blue solid arrows) and angular, semicircular canal acceleration components (red solid arrow) are indicated; magenta dashed arrows represent the resulting centripetal linear component during out-axis rotation. α, Θ, angular displacement between *tn-1* and *tn*.

STAR★Methods

KEY RESOURCES TABLE

REAGENT or RESOURCE	SOURCE	IDENTIFIER
Chemicals, Peptides, and Recombinant Proteins		
MS-222	Sigma-Aldrich, France	886-86-2
Hyaluronidase	Sigma-Aldrich, France	H1136-1AMP
Deposited Data		
Raw data and videos	This paper, Mendeley data	Mendeley dataset CURRENT-BIOLOGY-D-19-01330 http://dx.doi.org/10.17632/gn6pnsnkvm.1
Experimental Models: Organisms/Strains		
Xenopus laevis larva	Centre de Ressources Biologiques Xénopes, UMS 3387, CNRS, Rennes France	N/A
Software and Algorithms		
Software	This paper, mendeley data	Mendeley dataset CURRENT-BIOLOGY-D-19-01330 http://dx.doi.org/10.17632/gn6pnsnkvm.1
MATLAB2014b, 2018a MathWorks https://www.mathworks.com/products/ matlab.html	MATLAB2014b, 2018a MathWorks https://www.mathworks.com/products/ matlab.html	MATLAB2014b, 2018a MathWorks https://www.mathworks.com/products/ matlab.html
CED 1401, Signal, Spike 2; Cambridge Electronic Design	Cambridge Electronic Design	http://ced.co.uk/products/spkovin
Dataview	St-Andrew University	https://www.st-andrews.ac.uk/~wjh/dataview/
Custom-build software with Python 3.5	IMAGYS core facility INCIA CNRS UMR 5287	http://www.incia.u-bordeaux1.fr/spip.php?article629
Other		
Digital camera MemView	MemView, Southern Vision Systems Inc., USA	N/A
60mm lens 1:2.8D, and 50mm lens 1:1.8D lens AF NIKKOR,	Nikon, Japan	https://www.nikon.com/
Digital camera Basler ac1920	Basler AG An der Strusbek 60 – 62 22926 Ahrensburg Germany	https://www.baslerweb.com/en/
Optem MVZL macro video zoom lens, QIOPTIQ	QIOPTIQ	http://www.qioptiq.com/

LEAD CONTACT AND MATERIALS AVAILABILITY

Further information and requests for resources should be directed to and will be fulfilled by the Lead Contact, François Lambert (François.Lambert@u-bordeaux.fr). This study did not generate unique reagents.

EXPERIMENTAL MODEL AND SUBJECT DETAILS

Animals were obtained from an authorized supplier (Centre de Ressources Biologiques *Xénopes*, UMS 3387, CNRS, Rennes France) and kept in the laboratory in filtered water at 18°C until use for experimentation. Experiments were conducted on *Xenopus laevis* tadpoles of either sex (n = 72) at developmental stages 47, 50, 52 and 57 [40] and complied with the "Principles of Animal Care", publication No. 86-23, revised 1985 by the National Institute of Health. Experimental protocols were approved by the local ethical committee for animal research at the Université Paris Descartes (#3301100012-A) and the University of Bordeaux (#2016011518042273 APAFIS #3612).

METHOD DETAILS

Anatomical landmarks for motion tracking

To faithfully track head and concurrent eye movements during free swimming in *Xenopus* tadpoles (see Figure 1), animals were subjected to a topographic mapping of selected anatomical markers prior to the conduction of behavioral experiments. The position of both eyes and otic capsules (OC, inner ears) in the head as well as the heart as a reference for the center of the body was determined in each animal (Figure S1A). These parameters allowed triangulation of the anatomical distances between the eyes and the center of the OCs and their positions relative to each other and to the heart. To obtain these reference markers, tadpoles were anesthetized in 0.03% 3-aminobenzoic acid ethyl ester (MS-222; Pharmaq Ltd., Fordingbridge, Hampshire, UK) in water. Animals were secured to the bottom of a small petri dish and images were taken from the dorsal and ventral side (MemView Camera, Southern Vision Systems Inc., USA; 60 mm lens 1:2.8D, AF NIKKOR, Nikon, Japan; Resolution: 1024 x 1024 pixels; Figure S1A). Images were processed off-line using analysis software (ImageJ) to determine the distances between the different anatomical markers in stage 47 (n = 24) and stage 57 tadpoles (n = 20; table 1). To compensate for potential inter-individual variations in body size, data were normalized to the inter-ocular distance. This procedure showed that the relative distance between the otic capsules and the heart or the eyes and the otic capsules is very similar at both developmental stages (Table 1; Figure S1B). Based on the better view of the eyes from the ventral side, swimming episodes were video-tracked with the camera positioned underneath the tank (Figure S1C). The reconstruction of head and eye movements and the position of both OCs by automated off-line analyses (see below) were performed on the basis of the pre-determined distances of the respective anatomical structures prior to the video tracking (Figure S1A).

Anatomical feature	**Stage 47 (in mm)**	**Stage 47 (normalized)**	**Stage 57 (in mm)**	**Stage 57 (normalized)**
Eye-Eye	4.1 +/-0.4	1	9.4 +/-0.4	1
Otic capsule-Heart	1.3 +/-0.2	0.4	3.4 +/-0.4	0.38
Eye-otic capsule	2.1 +/-0.3	0.53	4.6 +/-0.6	0.52
Eye-Heart	2.8 +/-0.3	0.68	5.3 +/-0.02	0.57

Anatomical feature table: Anatomical features were studied in stage 47 (n = 24) and stage 57 tadpoles (n = 20). Distances between the different anatomical markers shown in Figure S1B are reported in mm for stage 47 (first column) and stage 57 (third column), and normalized to the individual inter-ocular distance (second and fourth column for stage 47 and 57, respectively). Note that the relative distance between the otic capsules and the heart or the eyes and the otic capsules is constant despite the body growth.

High-speed video tracking of swimming episodes

Tracking of swimming episodes and eye movements was performed in two complementary recording sessions: a first set of experiments aimed at high spatial and temporal resolution of swimming sequences in order to track eye movements during free swimming. A second set of experiments aimed at tracking the motion kinematics during longer swimming episodes. Accordingly, the motion kinematics of the head, eye and heart in space during free swimming was studied in animals (stage 47, n = 24; stage 57, n = 20) that were placed in a Plexiglas tank (5 x 25 cm) with a water depth of 5 cm. Video sequences were recorded with a digital camera (MemView, Southern Vision Systems Inc., USA), positioned underneath the tank (Figure S1C). Eye movements were tracked by placing the camera as close as possible to the ventral surface of the tank to restrain the field of view and to increase the spatial resolution. A 60 mm lens (1:2.8D, AF NIKKOR, Nikon, Japan) was used to monitor magnified views of the animals. A wide-angle lens (50 mm 1:1.8D lens AF NIKKOR, Nikon, Japan) was used to capture longer swimming episodes and to extract the kinematics of swimming-related head movements. Light sources (Barefly 200, KINOFLO Lighting system; Figure S1A) were placed underneath the

tank and oriented such that variations in light reflections were minimal. A second light source (LED LitePad HO (15 x 30 cm, Rosco, USA) was placed above the pool to provide a homogeneous white illuminated background (Figure S1C). To account for size differences between animals at stage 47 and 57 [19], the distance between camera and tank was adjusted to maintain a similar relative image size of the animal (determined by the inter-ocular distance). Eye and head movements were recorded during separate swimming episodes at an image acquisition rate of 750 and 250 frames per seconds (fps), respectively. Swimming episodes lasted for up to 20 tail oscillations (Figure S1D). Only uninterrupted episodes of free swimming that consisted of at least 5 consecutive cycles of tail undulations were further analyzed. The analysis was restricted to swimming episodes that occurred in the horizontal plane, i.e. without concurrent roll motion. Head/body roll movements during swimming were detected in the video recordings by calculating the distance between the two eyes. Episodes in which the individual, pre-determined inter-ocular distance cyclically varied by more than 1% (corresponding to ~8° vertical oscillations of the head) due to roll movements were excluded from the analysis. See videos S1 and S2 (also deposited at http://dx.doi.org/10.17632/gn6pnsnkvm.1)

Video recordings and analysis of eye movements in mechanically secured semi-intact head preparations

Experiments on semi-intact head preparations served to isolate otolith-related eye movements during specific motion stimulation paradigms. All procedures were performed according to the protocol by Bacqué-Cazenave et al. [11]. In brief, *Xenopus* larvae at stage 47 (n = 5) were anesthetized in a 0.05% MS-222 solution and placed in oxygenated (95% O_2, 5% CO_2) Ringer solution. The temperature of the bath solution was maintained at 18°C. Viscera and forebrain were removed, the brainstem was exposed to give access to the Ringer solution and the tail was removed at the level of the upper spinal cord. To abolish visual sensory inputs, both optic nerves were transected and the semi-intact preparation was firmly secured onto the Sylgard floor of a chamber with insect pins.

The chamber with the preparation was mounted onto a computer-controlled, motorized motion stimulation device that allowed placement of the recording chamber either in the center or at off-center positions with respect to the vertical axis of the stimulator (turntable and sled, Technoshop COH@BIT, IUT de Bordeaux, University of Bordeaux). Motion stimuli consisted of sinusoidal translations at 1 Hz ±25 mm along the transverse axis, or of sinusoidal rotations at a frequency of 1 Hz and peak stimulus velocities that ranged from ±30°/s to ±240°/s with the rotation axis either centered between the two OCs or located laterally outside the head (5 mm).

Left- and rightward directed eye movements were video-recorded from top at 200 fps with a high-speed digital camera (Basler, ac1920) equipped with a micro-inspection lens system (Optem MVZL macro video zoom lens, QIOPTIQ). Automatic tracking of eye motion segments was performed using a custom-built software written in Python 3.5 environment (IMAGYS core facility, INCIA UMR CNRS 5287). For eye movement measurements, a ROI was drawn around each eye and a binary threshold was applied before tracking the angle between the minor axis of the eye ellipse and the head axis. See videos S3 and S4 (also deposited at http://dx.doi.org/10.17632/gn6pnsnkvm.1)

Raw data from video recordings were processed off-line and analyzed with Dataview (by W.J. Heitler, University of St Andrews, Scotland). For video image processing, traces of angular movements of the eyes were first filtered with a 25 Hz low-pass filter. Thereafter, maximal angular excursions of the eyes (peak sinewave) were detected for each individual motion cycle and used to calculate the amplitude of eye movements.

Injection of MS-222 or hyaluronidase in the bilateral otic capsule

After video recordings of eye movements in stage 47 semi-intact head preparation under control conditions (n = 6; see Figure 3A), a calibrated 10 nl volume of a 0.5% MS-222 solution dissolved in artificial endolymph Ringer solution [10,41] was injected into both otic capsules, respectively. The injection was performed by inserting a beveled microelectrode (30°, 10-15 µm tip diameter; GB150F-8P, Science Products GmbH, Germany) inserted into the center of the transparent otic capsule with a micromanipulator under visual control. The calibrated volume of 10 nl was pressure-injected (0.5 bar, 5 s) with a PICOSPRITZER III pressure injector (Intracel, UK). To prevent the developmental formation of semicircular canals on both sides, a previous established method was employed [16-18]. Accordingly, a calibrated volume (10 nl) of a hyaluronidase enzyme solution (0.5 mg/ml, Sigma-Aldrich, France), dissolved in artificial endolymph Ringer solution was injected into bilateral otic capsules of tadpoles at stage 44 (n = 5). Subsequently, animals were allowed to develop into older stages.

Electrophysiological recording of extraocular motor nerve spike discharge

Recording of extraocular motor nerve activity was performed *in vitro* in semi-intact preparations of stage 50 (n = 4) *Xenopus* tadpoles as described previously [10, 23]. In brief, animals were deeply anesthetized in a cold (4-6°C) solution of 0.05% MS-222 in frog Ringer (75 mM NaCl, 25 mM $NaHCO_3$, 2 mM $CaCl_2$, 2 mM KCl, 0.5 mM $MgCl_2$, and 11 mM glucose, pH 7.4) and decapitated at the level of the upper spinal cord. The skin covering the dorsal region of the head was removed, the soft skull tissue opened and the forebrain disconnected. This surgical procedure anatomically preserved the remaining central nervous system, bilateral inner ear endorgans in the OCs including the VIIIth nerves as well as the extraocular motor nerves and eye muscle innervations [10]. After selective disconnection of the abducens nerve from the lateral rectus (LR) target muscle, preparations were transferred to a Sylgard-lined Petri dish (volume 5 ml), and continuously superfused with oxygenated Ringer solution at a rate of 1.5 - 2.1 ml/min and a temperature of 17°C ± 0.1°C.

Multi-unit spike discharge of the LR nerve was recorded with glass suction microelectrodes, produced with a horizontal puller (P-87 Brown/Flaming, Sutter Instruments Company, Novato, CA, USA). Electrode tips were broken and individually adjusted to fit the LR nerve diameter. Natural activation of vestibular endorgans was performed with a computer-controlled, motorized two-axis turntable (ACT-1002, Acutronic USA Inc., Switzerland) as described previously [10, 23]. The recording chamber with the preparation was mounted onto a custom-built plate that allowed placement of the recording chamber either in the center or at off-center positions with respect to the vertical axis of the turntable. Accordingly, the rotational axis was either centered between the two OCs or located laterally outside the head. This configuration allowed recordings of LR nerve spike discharge during centered or off-center vertical-axis head rotations. Motion stimuli consisted of sinusoidal oscillations at a frequency of 1 Hz and a peak stimulus velocity that ranged from ±30°/s to ±240°/s. Spontaneous and evoked multi-unit LR nerve spike discharges were recorded (Ext 10-2F; npi Electronics, Tamm, Germany), digitized (10 kHz), stored on a computer and analyzed off-line (CED 1401, Signal, Spike 2; Cambridge Electronic Design). The magnitude of the discharge modulation was determined by calculating the difference between minimum and maximum firing rates of the averaged discharge over a single turntable motion cycle [10].

QUANTIFICATION AND STATISTICAL ANALYSIS

Analysis of head and otic capsule (inner ear) kinematics

Custom image processing and analysis software was developed in Matlab to track head and eye movements in video recordings and to determine 2-D spatial positions (X-Y coordinates) of the left and right eye based on a frame-by-frame analysis with the Video Spot Tracker 5.3 (credit: CISMM at UNC-CH; see acknowledgments). Predetermined anatomical landmarks (see above; Supplemental table 1) were used to calculate the 2-D position of the heart as well as the position of the left and right OCs with respect to the X-Y coordinates of the heart and eyes (Figure S1D).

The trajectories of four anatomical markers (head, heart, left and right OC) were further analyzed in Matlab to provide relevant kinematic variables (curvature of head trajectories; acceleration magnitudes of heart, eyes and OCs) that represent the animals' motion trajectory and swimming performance. A non-uniform circular mobile point kinematic model was used to describe the curved trajectories of the landmarks (Figure S1D). In this model, the trajectory of a moving point was decomposed into series of local circular trajectories (Figure S1E), defined by a particular center and radius calculated for each video frame. This kinematic model allowed distinguishing forward, lateral, centripetal and angular components of the acceleration profile for both OCs during off-center head movements produced by undulatory tail-based swimming.

High-speed video recordings and analysis of eye movements during episodes of free swimming

Sequences of individual images were analyzed off-line using a custom Matlab script. Tracking of the eyes and calculation of head-in-space and eye-in-space angular positions were performed using a semi-automatic frame-by-frame analysis as described previously [42]. Briefly, a region of interest (ROI) was drawn around each eye and processed using binary thresholding. This made the eyeball and lens to appear as two distinct black/white morphological structures. The position of each eye in space was computed as the orientation of the major axis of an ellipse, which approximates the outline of the eye [42]. The position of the head-in-space was obtained from the angle of the inter-ocular connection line between the two eyes. These values served to estimate the efficiency of compensatory eye movements during concurrent swimming-related head movements. Accordingly, the magnitude of the eye motion with respect to the head motion was determined as the ratio between the eye-in-space angle and the head-in-space angle.

Statistics

Free swimming kinematic values generated in CSV files obtained from Matlab were analyzed using OriginPro 8 (OriginLab Corporation, USA). Data are presented as mean ± standard error of the mean (SEM)

unless stated otherwise. For whisker box plots shown in Figure 1G and Figure 2H,I, black circles represent 1% and 99%, respectively; black bowls represent the mean, error bars are ±SEM. Non-parametric unpaired Mann-Whitney *U*-test was used to determine significant differences between mean values (detailed statistical descriptions are provided in the respective result section and corresponding figure legends). Non-parametric Kolmogorov-Smirnov test was used to determine significant differences between data distribution (detailed statistical descriptions are provided in the respective result section and corresponding figure legends). Statistical tests were performed with Prism 7.0 (GraphPad). Eye/head motion phase relationships were calculated with Oriana 4.02 (Kovach computing services, UK).

DATA AND CODE AVAILABILITY

The accession number for the original videos and datasheets and experimental software generated through this study have been deposited to Mendeley dataset CURRENT-BIOLOGY-D-19-01330 (http://dx.doi.org/10.17632/gn6pnsnkvm.1)

SUPPLEMENTAL VIDEOS

Video S1. Video sequence of free swimming stage 47 larva. Related to Figure 2

Video S2. Video sequence of free swimming stage 57 larva. Related to Figure 2

Video S3. Video sequence of stage 47semi-intact head preparation during lateral translation. Related to Figure 3

Video S4. Video sequence of stage 47semi-intact head preparation during out-axis rotation. Related to Figure 3

High resolution versions of supplemental videos are available at http://dx.doi.org/10.17632/gn6pnsnkvm.1

REFERENCES

1. Straka, H. (2010). Ontogenetic rules and constraints of vestibulo-ocular reflex development. Curr. Opin. Neurobiol. *20*, 689-95.
2. Bagnall, M.W., Schoppik, D. (2018). Development of vestibular behaviors in zebrafish. Curr. Opin. Neurobiol. *53*, 83-89.
3. Glover, J.C. (2003). The development of vestibulo-ocular circuitry in the chicken embryo. J. Physiol. Paris. *97*, 17-25.
4. Wolf, S., Dubreuil, A.M., Bertoni, T., Böhm, U.L., Bormuth, V., Candelier, R., Karpenko, S., Hildebrand, D.G.C., Bianco, I.H., Monasson, R., Debrégeas, G. (2017). Sensorimotor computation underlying phototaxis in zebrafish. Nat. Commun. *8*, 651.
5. Migault, G., van der Plas, T.L., Trentesaux, H., Panier, T., Candelier, R., Proville, R., Englitz, B., Debrégeas, G., Bormuth, V. (2018). Whole-Brain Calcium Imaging during Physiological Vestibular Stimulation in Larval Zebrafish. Curr. Biol. *28*, 3723-3735.e6
6. Bianco, I.H., Ma, L.H., Schoppik, D., Robson, D.N., Orger, M.B., Beck, J.C., Li, J.M., Schier, A.F., Engert, F., Baker, R. (2012). The tangential nucleus controls a gravito-inertial vestibulo-ocular reflex. Curr. Biol. *22*, 1285-95.
7. Favre-Bulle, I.A., Vanwalleghem, G., Taylor, M.A., Rubinsztein-Dunlop, H., Scott, E.K. (2018). Cellular-Resolution Imaging of Vestibular Processing across the Larval Zebrafish Brain. Curr. Biol. *28*, 3711-3722.e3.
8. Horn, E., Lang, H.G., Rayer, B. (1986). The development of the static vestibulo-ocular reflex in the southern clawed toad, Xenopus laevis. I. Intact animals. J. Comp. Physiol. A. *159*, 869-78.
9. Beck, J.C., Gilland, E., Tank, D.W., Baker, R. (2004) Quantifying the ontogeny of optokinetic and vestibuloocular behaviors in zebrafish, medaka, and goldfish. J. Neurophysiol. *92*, 3546-61.
10. Lambert, F.M., Beck, J.C., Baker, R. and Straka, H. (2008). Semicircular canal size determines the developmental onset of angular vestibuloocular reflexes in larval *Xenopus*. J. Neurosci. *28*, 8086-8095.
11. Bacqué-Cazenave, J., Courtand, G., Beraneck, M., Lambert, F.M., Combes, D. (2018). Temporal relationship of ocular and tail segmental movements underlying locomotor-induced gaze stabilization during undulatory swimming in larval *Xenopus*. Front. Neural Circuits. *29*, 12:95.
12. Mo, W., Chen, F., Nechiporuk, A., Nicolson, T. (2010). Quantification of vestibular-induced eye movements in zebrafish larvae. BMC Neurosci. *11*, 110.

13. Favre-Bulle, I.A., Stilgoe, A.B., Rubinsztein-Dunlop, H., Scott, E.K. (2017). Optical trapping of otoliths drives vestibular behaviours in larval zebrafish. Nat. Commun. *8*, 630.
14. Straka, H. and Dieringer, N. (2004). Basic organization principles of the VOR: lessons from frogs. Prog. Neurobiol. *73*, 259-309.
15. Ramlochansingh, C., Branoner, F., Chagnaud, B.P., Straka, H. (2014). Efficacy of tricaine methanesulfonate (MS-222) as an anesthetic agent for blocking sensory-motor responses in Xenopus laevis tadpoles. PLoS One. *9*, e101606.
16. Haddon, C.M., Lewis, J.H. (1991). Hyaluronan as a propellant for epithelial movement: the development of semicircular canals in the inner ear of Xenopus. Development. *112*, 541-50.
17. Branoner, F., Straka, H. (2015). Semicircular canal-dependent developmental tuning of translational vestibulo-ocular reflexes in Xenopus laevis. Dev. Neurobiol. *75*, 1051-67.
18. Branoner, F., Straka, H. (2018). Semicircular Canal Influences on the Developmental Tuning of the Translational Vestibulo-Ocular Reflex. Front. Neurol. *9*, 404.
19. Hänzi, S. and Straka, H. (2017). Developmental changes in head movement kinematics during swimming in Xenopus laevis tadpoles. J. Exp. Biol. *220*, 227-236.
20. Liu, H., Wassersug, R., Kawachi, K. (1996). A computational fluid dynamics study of tadpole swimming. J. Exp. Biol. *199*, 1245-60.
21. Chagnaud, B.P., Simmers, J. and Straka, H. (2012). Predictability of visual perturbation during locomotion: implications for corrective efference copy signaling. Biol. Cybern. *106*, 669-679.
22. Straka, H., Simmers, J., Chagnaud, B.P. (2018). A New Perspective on Predictive Motor Signaling. Curr. Biol. *28*, R232-R243.
23. Lambert, F.M., Combes, D., Simmers, J. and Straka, H. (2012). Gaze stabilization by efference copy signaling without sensory feedback during vertebrate locomotion. Curr. Biol. *22*, 1649-58.
24. Bacque-Cazenave, J., Lambert, F.M., Cayrel, M., Courtand, G., Beraneck, M., and Combes, D. (2017). "Quantifying the spinal locomotor network-driven oculomotor behavior and its developmental adaptation in frog," in Proceedings of the Annual Meeting of Society for Neuroscience, Washington, DC.
25. Sillar, K.T., Wedderburn, J.F., Simmers, A.J. (1991). The development of swimming rhythmicity in post-embryonic Xenopus laevis. Proc. Biol. Sci. *246*, 147-53.
26. Straka, H., Holler, S., Goto, F. (2002). Patterns of canal and otolith afferent input convergence in frog second-order vestibular neurons. J. Neurophysiol. *88*, 2287-301.
27. Bush, G.A., Perachio, A.A., Angelaki, D.E. (1993). Encoding of head acceleration in vestibular neurons. I. Spatiotemporal response properties to linear acceleration. J. Neurophysiol. *69*, 2039-55.
28. Uchino, Y., Sasaki, M., Sato, H., Bai, R., Kawamoto, E. (2005). Otolith and canal integration on single vestibular neurons in cats. Exp. Brain. Res. *164*, 271-85.
29. Hess, B.J., Dieringer, N. (1991). Spatial organization of linear vestibuloocular reflexes of the rat: responses during horizontal and vertical linear acceleration. J. Neurophysiol. *66*, 1805-18.
30. Rohregger, M., Dieringer, N. (2002). Principles of linear and angular vestibuloocular reflex organization in the frog. J. Neurophysiol. *87*, 385-98.
31. Straka, H., Baker, R. (2013). Vestibular blueprint in early vertebrates. Front Neural Circuits. 7:182.
32. Ehrlich D.E., Schoppik, D. (2019). A primal role for the vestibular sense in the development of coordinated locomotion. Elife. *8*, e45839.
33. Fritzsch, B., Straka, H. (2014). Evolution of vertebrate mechanosensory hair cells and inner ears: toward identifying stimuli that select mutation driven altered morphologies. J. Comp. Physiol. A. Neuroethol Sens. Neural. Behav. Physiol. *200*, 5-18.
34. Muller, M. (1999). Size limitations in semicircular duct systems. J. Theor. Biol. *198*, 405– 437.
35. Rabbitt, R.D., Damiano, E.R., Grant, J.W. (2004). Biomechanics of the vestibular semicircular canals and otolith organs. In: The vestibular system (Highstein SM, Fay RR, Popper AN, eds), pp 153–201. New York: Springer.
36. Hullar, T.E. (2006). Semicircular canal geometry, afferent sensitivity, and animal behavior. Anat. Rec. .A Discov. Mol. Cell. Evol. Biol. *288*, 466–472.
37. Yang, A., Hullar, T.E. (2007). Relationship of semicircular canal size to vestibular-nerve afferent sensitivity in mammals. J. Neurophysiol. *98*, 3197–3205.
38. Angelaki, D.E. (1992). Vestibular neurons encoding two-dimensional linear acceleration assist in the estimation of rotational velocity during off-vertical axis rotation. Ann. N. Y. Acad. Sci. 656, 910-3.
39. Angelaki, D.E. (1992). Two-dimensional coding of linear acceleration and the angular velocity sensitivity of the otolith system. Biol. Cybern. *67*, 511-21.

40. Nieuwkoop, P.D., Faber, J. (1994). Normal table of *Xenopus laevis* (Daudin): a systematical and chronological survey of the development from the fertilized egg till the end of metamorphosis. New York: Garland.
41. Eatock, R.A., Corey, D.P., Hudspeth, A.J. (1987). Adaptation of mechanoelectrical transduction in hair cells of the bullfrog's sacculus. J. Neurosci. *7*, 2821-36.
42. von Uckermann, G., Lambert, F.M., Combes, D., Straka, H. and Simmers, J. (2016). Adaptive plasticity of spino-extraocular motor coupling during locomotion in metamorphosing Xenopus laevis. J. Exp. Biol. *219*, 1110-21.

CellPress

TABLE FOR AUTHOR TO COMPLETE

Please upload the completed table as a separate document. ***Please do not add subheadings to the Key Resources Table.*** *If you wish to make an entry that does not fall into one of the subheadings below, please contact your handling editor. (****NOTE:*** *For authors publishing in Current Biology, please note that references within the KRT should be in numbered style, rather than Harvard.)*

KEY RESOURCES TABLE CURRENT-BIOLOGY-D-19-01330

REAGENT or RESOURCE	SOURCE	IDENTIFIER
Antibodies		
none		
Bacterial and Virus Strains		
none		
Biological Samples		
none		
Chemicals, Peptides, and Recombinant Proteins		
MS-222	Sigma-Aldrich, France	886-86-2
Hyaluronidase	Sigma-Aldrich, France	H1136-1AMP
Critical Commercial Assays		
none		
Deposited Data		
Raw data and videos	This paper, Mendeley data	Mendeley dataset CURRENT-BIOLOGY-D-19-01330 http://dx.doi.org/10.17632/gn6pnsnkvm.1

Experimental Models: Cell Lines		
none		
Experimental Models: Organisms/Strains		
Xenopus laevis larva	Centre de Ressources Biologiques Xénopes, UMS 3387, CNRS, Rennes France	N/A
Oligonucleotides		
none		
Recombinant DNA		
none		
Software and Algorithms		
Software	This paper, mendeley data	Mendeley dataset CURRENT-BIOLOGY-D-19-01330 http://dx.doi.org/10.17632/gn6pnsnkvm.1
MATLAB2014b, 2018a MathWorks https://www.mathworks.com/products/matlab.html	MATLAB2014b, 2018a MathWorks https://www.mathworks.com/products/ matlab.html	MATLAB2014b, 2018a MathWorks https://www.mathworks.com/products/ matlab.html
CED 1401, Signal, Spike 2; Cambridge Electronic Design	Cambridge Electronic Design	http://ced.co.uk/products/spkovin
Dataview	St-Andrew University	https://www.st-andrews.ac.uk/~wjh/dataview/
Custom-build software with Python 3.5	IMAGYS core facility INCIA CNRS UMR 5287	http://www.incia.u-bordeaux1.fr/spip.php?article629
Other		
Digital camera MemView	MemView, Southern Vision Systems Inc., USA	N/A

60mm lens 1:2.8D, and 50mm lens 1:1.8D lens AF NIKKOR,	Nikon, Japan	https://www.nikon.com/
Digital camera Basler ac1920	Basler AG An der Strusbek 60 – 62 22926 Ahrensburg Germany	https://www.baslerweb.com/en/
Optem MVZL macro video zoom lens, QIOPTIQ	QIOPTIQ	http://www.qioptiq.com/

Figure 1

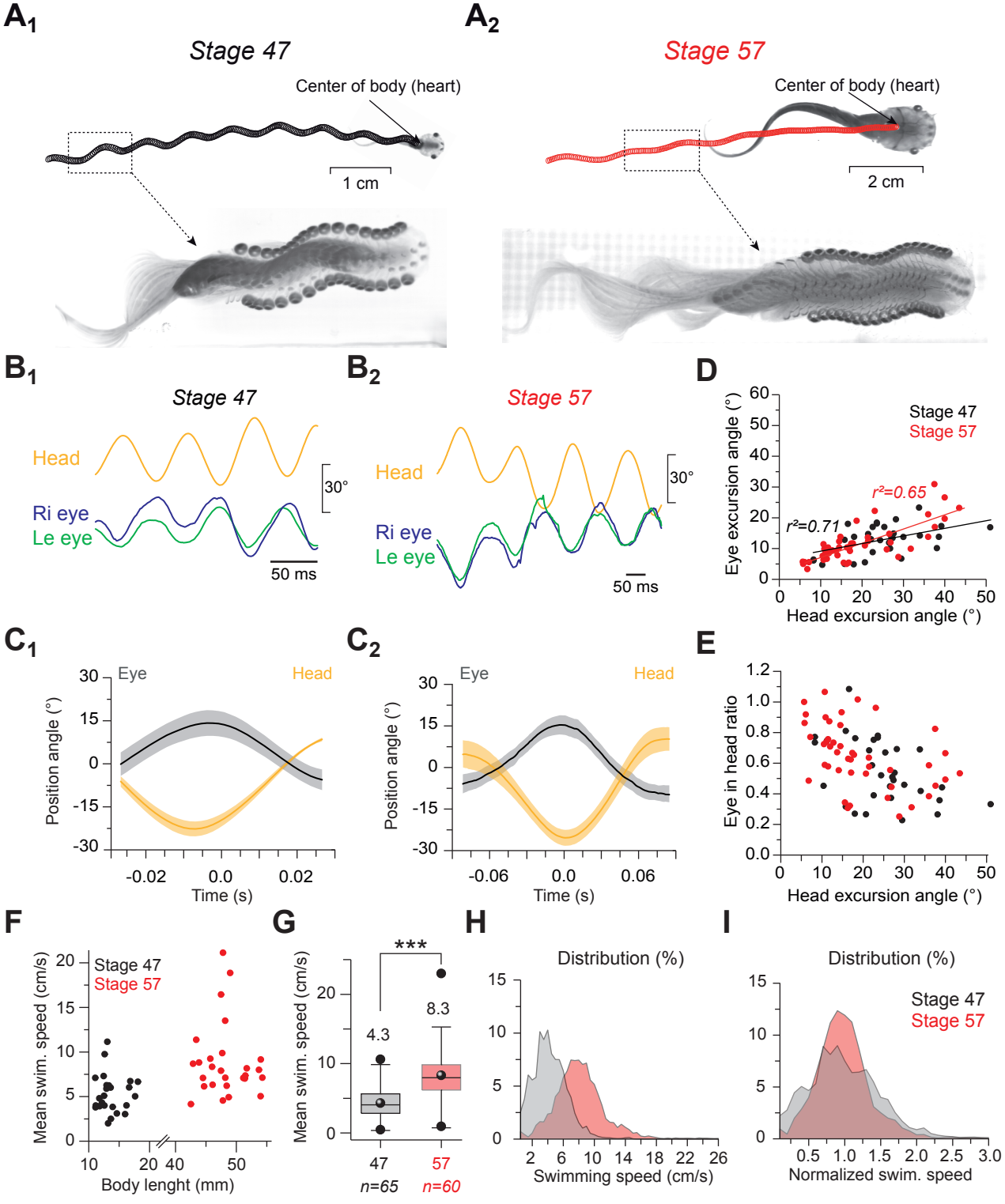
A1
Stage 47
Center of body (heart)
1 cm
A2
Stage 57
Center of body (heart)
2 cm
B1
Stage 47
Head
Ri eye
Le eye
30°
50 ms
B2
Stage 57
Head
Ri eye
Le eye
30°
50 ms
D
Stage 47
Stage 57
r²=0.65
r²=0.71
Eye excursion angle (°)
Head excursion angle (°)
C1
Eye
Head
Position angle (°)
Time (s)
C2
Eye
Head
Position angle (°)
Time (s)
E
Eye in head ratio
Head excursion angle (°)
F
Stage 47
Stage 57
Mean swim. speed (cm/s)
Body lenght (mm)
G
***
4.3
8.3
Mean swim. speed (cm/s)
47
57
n=65
n=60
H
Distribution (%)
Swimming speed (cm/s)
I
Distribution (%)
Stage 47
Stage 57
Normalized swim. speed

Figure 2

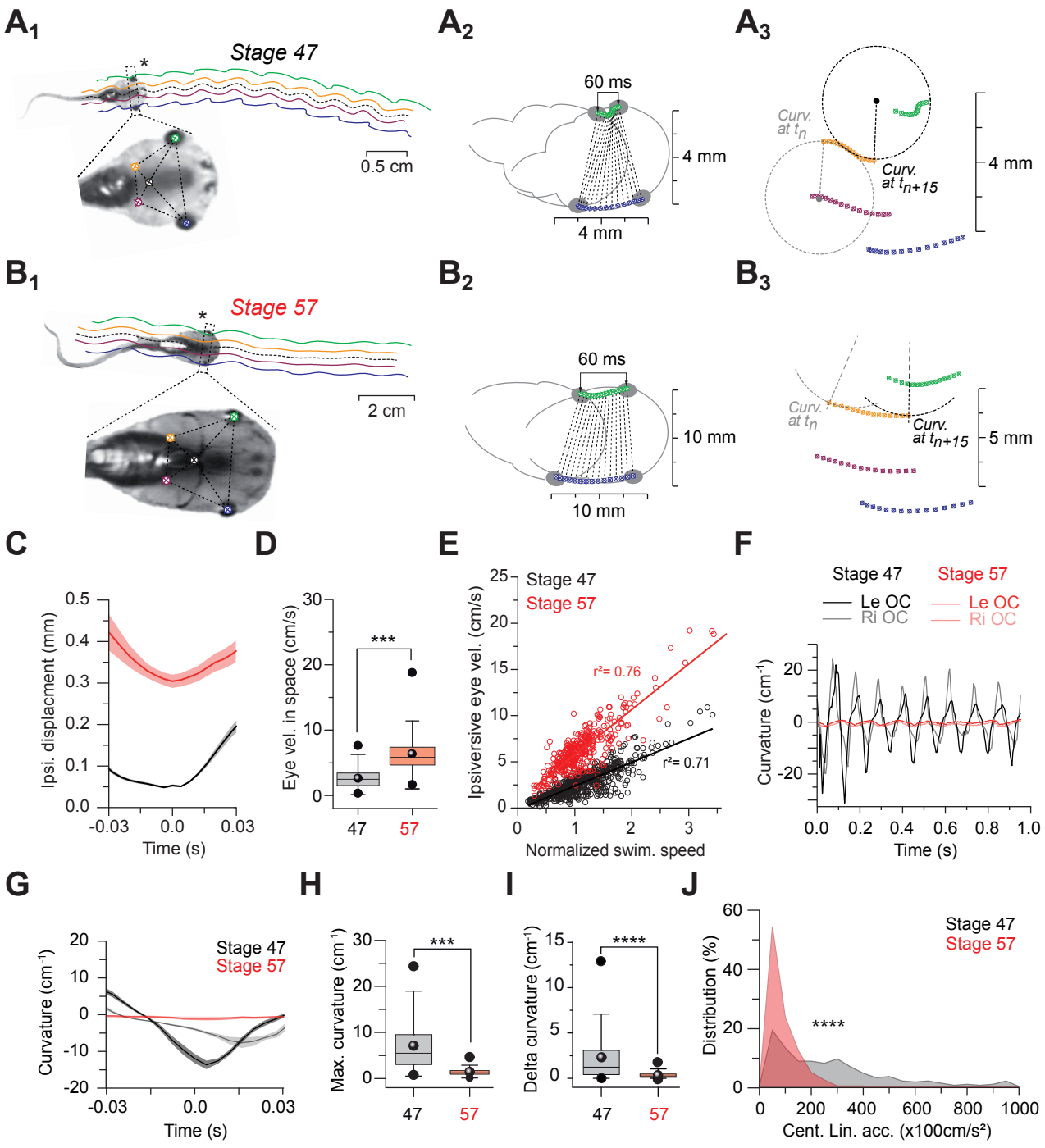
A1
Stage 47
0.5 cm
A2
60 ms
4 mm
4 mm
A3
Curv. at t_n
Curv. at t_{n+15}
4 mm
B1
Stage 57
2 cm
B2
60 ms
10 mm
10 mm
B3
Curv. at t_n
Curv. at t_{n+15}
5 mm
C
Ipsi. displacment (mm)
Time (s)
D
Eye vel. in space (cm/s)
***
47
57
E
Stage 47
Stage 57
Ipsiversive eye vel. (cm/s)
r²= 0.76
r²= 0.71
Normalized swim. speed
F
Stage 47
Stage 57
Le OC
Ri OC
Le OC
Ri OC
Curvature (cm⁻¹)
Time (s)
G
Stage 47
Stage 57
Curvature (cm⁻¹)
Time (s)
H
Max. curvature (cm⁻¹)
***
47
57
I
Delta curvature (cm⁻¹)
****
47
57
J
Stage 47
Stage 57
Distribution (%)
****
Cent. Lin. acc. (x100cm/s²)

Figure 3

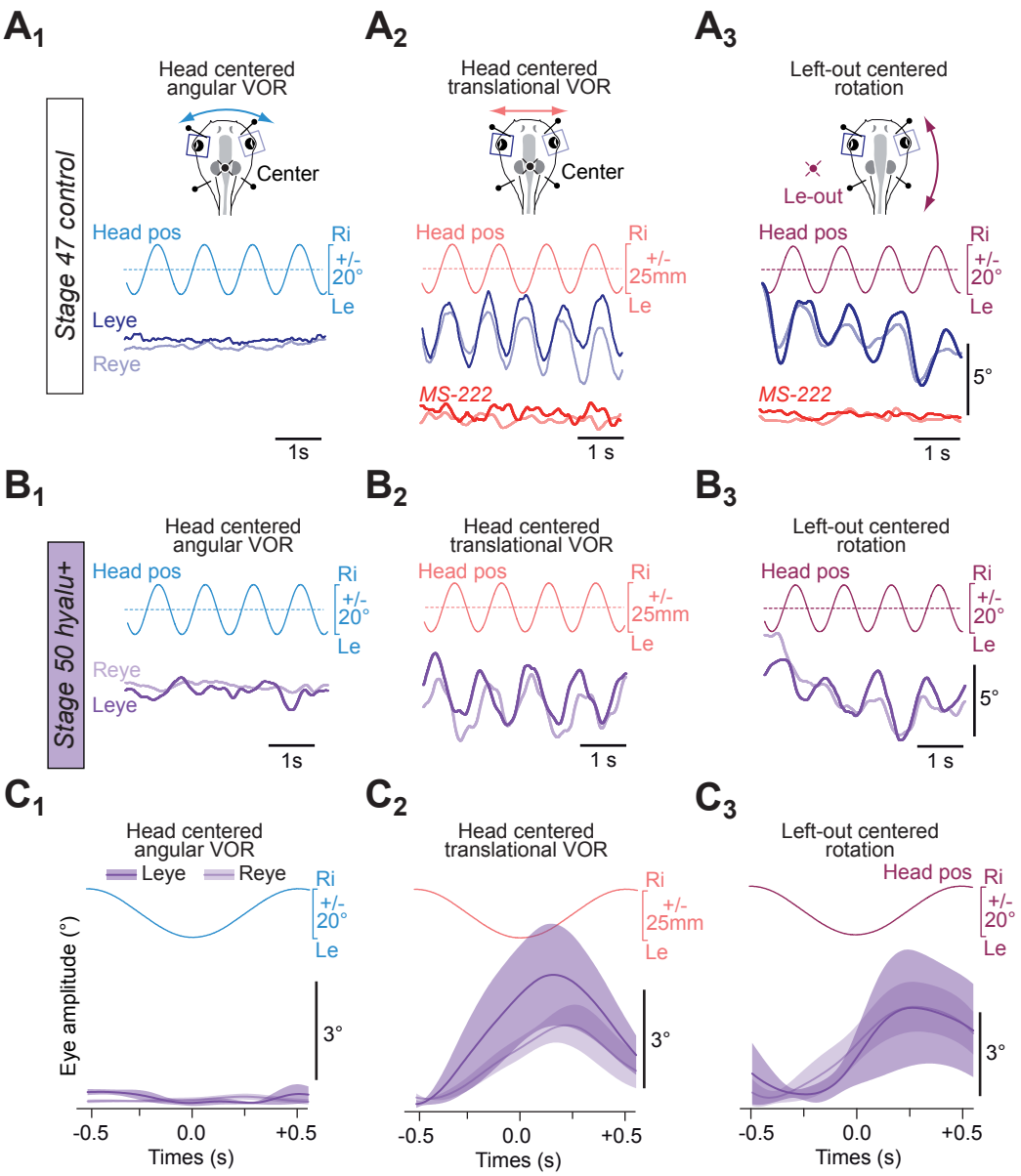
A1
Head centered angular VOR
Stage 47 control
Center
Head pos
Ri
+/- 20°
Le
Leye
Reye
1s
A2
Head centered translational VOR
Center
Head pos
Ri
+/- 25mm
Le
MS-222
1 s
A3
Left-out centered rotation
Le-out
Head pos
Ri
+/- 20°
Le
5°
MS-222
1 s
B1
Head centered angular VOR
Stage 50 hyalu+
Head pos
Ri
+/- 20°
Le
Reye
Leye
1s
B2
Head centered translational VOR
Head pos
Ri
+/- 25mm
Le
1 s
B3
Left-out centered rotation
Head pos
Ri
+/- 20°
Le
5°
1 s
C1
Head centered angular VOR
Leye
Reye
Ri
+/- 20°
Le
Eye amplitude (°)
3°
-0.5
0.0
+0.5
Times (s)
C2
Head centered translational VOR
Ri
+/- 25mm
Le
3°
-0.5
0.0
+0.5
Times (s)
C3
Left-out centered rotation
Head pos
Ri
+/- 20°
Le
3°
-0.5
0.0
+0.5
Times (s)

Figure 4

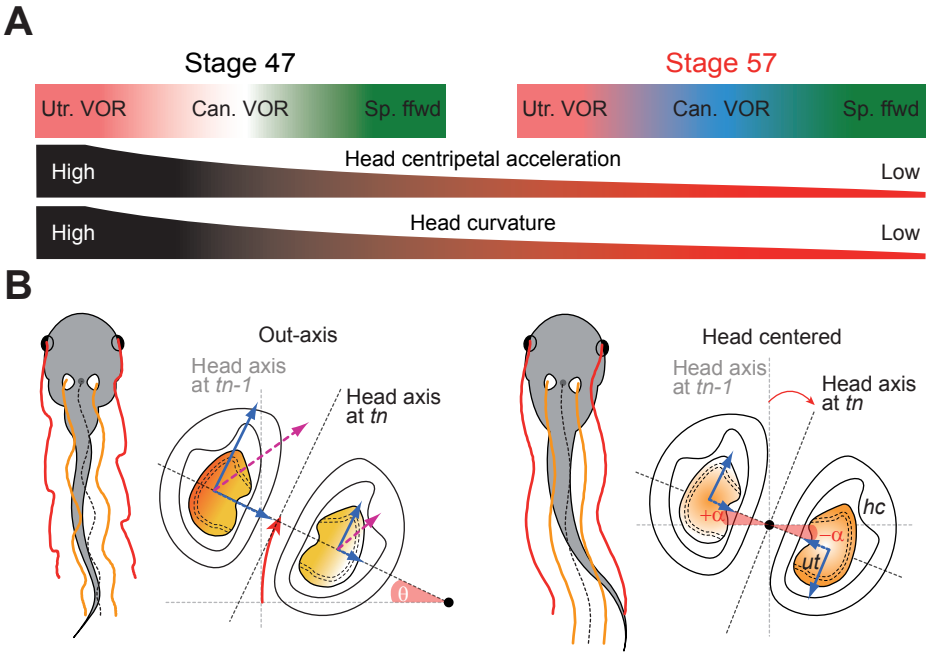
A
Stage 47
Utr. VOR
Can. VOR
Sp. ffwd
Stage 57
Utr. VOR
Can. VOR
Sp. ffwd
High
Head centripetal acceleration
Low
High
Head curvature
Low
B
Out-axis
Head axis at tn-1
Head axis at tn
θ
Head centered
Head axis at tn-1
Head axis at tn
+α
−α
hc
ut

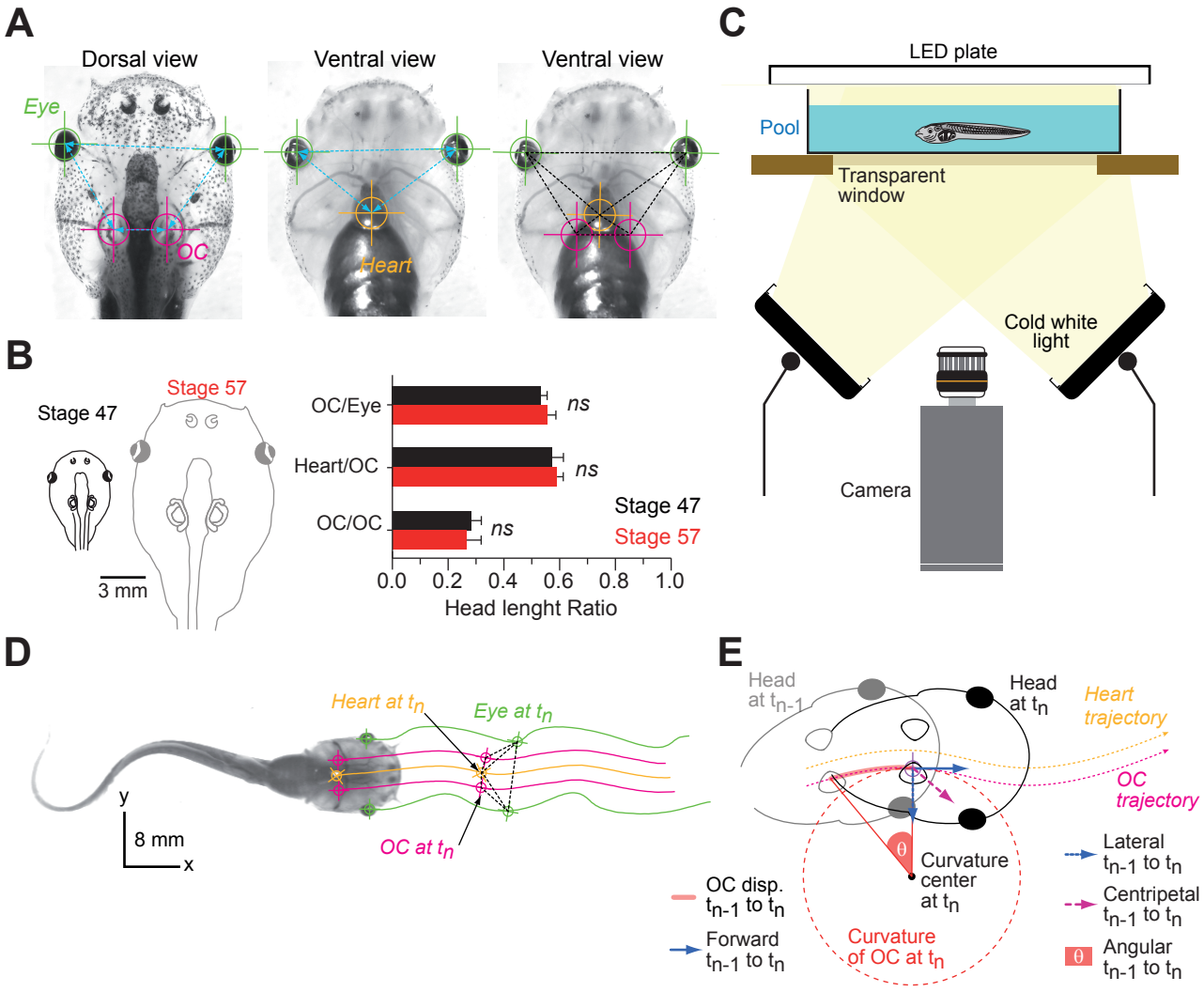
A
Dorsal view
Ventral view
Ventral view
Eye
OC
Heart
B
Stage 47
Stage 57
3 mm
OC/Eye
Heart/OC
OC/OC
ns
ns
ns
Stage 47
Stage 57
0.0 0.2 0.4 0.6 0.8 1.0
Head lenght Ratio
C
LED plate
Pool
Transparent window
Cold white light
Camera
D
Heart at t_n
Eye at t_n
OC at t_n
y
8 mm
x
E
Head at t_{n-1}
Head at t_n
Heart trajectory
OC trajectory
θ
Curvature center at t_n
Curvature of OC at t_n
OC disp. t_{n-1} to t_n
Forward t_{n-1} to t_n
Lateral t_{n-1} to t_n
Centripetal t_{n-1} to t_n
Angular t_{n-1} to t_n

Figure S1. Morphometric analysis of anatomical features and off-line calculation of head motion kinematic parameters. Related to Figure 1 and 2.

(A) Images depicting dorsal (left) and ventral views (middle, right) of a stage 57 larvae with outlined locations and measured or triangulated relative distances between eyes (green), heart (orange) and otic capsules (OC, magenta); anatomical markers served subsequently as landmarks for tracking the head motion during swimming.

(B) Scaled drawings of the head/body at stage 47 and 57 (left) and morphometric ratios of measured or calculated anatomical markers (right); note that despite size differences, relative distances between eyes, heart, OC remain constant during development, *ns*, not significant (Mann-Whitney *U*-test).

(C) Schematic of the set-up for high speed (500 fps) video recordings of free swimming.

(D) Ventral view of video imaged swimming of a stage 57 tadpole depicting the tracked trajectories of both eyes (green) and the triangulated heart (orange) and OCs (magenta) at the time point *tn*.

(E) Schematic summarizing the trajectory of the triangulated motion of the OC along with the direction and size of the forward, lateral, centripetal and angular acceleration vectors calculated from the displacement (disp.) between time point *tn-1* (gray) and time point *tn* (black); Θ, angular displacement.

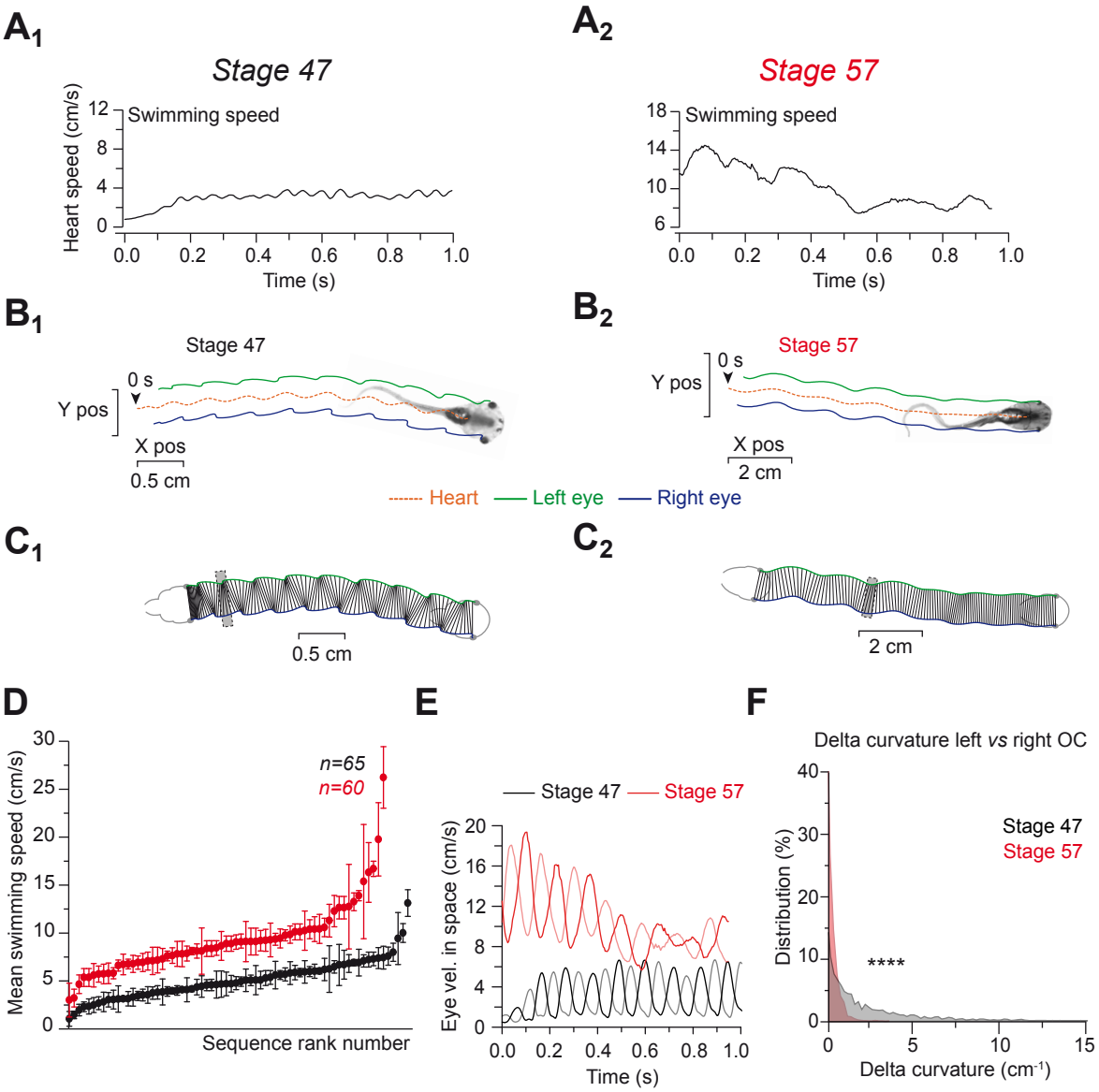
A1
Stage 47
Heart speed (cm/s)
Swimming speed
Time (s)
A2
Stage 57
Swimming speed
Time (s)
B1
Stage 47
Y pos
0 s
X pos
0.5 cm
B2
Stage 57
Y pos
0 s
X pos
2 cm
Heart
Left eye
Right eye
C1
0.5 cm
C2
2 cm
D
n=65
n=60
Mean swimming speed (cm/s)
Sequence rank number
E
Stage 47
Stage 57
Eye vel. in space (cm/s)
Time (s)
F
Delta curvature left vs right OC
Stage 47
Stage 57
Distribution (%)
****
Delta curvature (cm-1)

Figure S2. Comparison of swimming speed. Related to Figure 2.

(A, B and C) Instantaneous swimming speed (A1 and A2) obtained from the extracted trajectory of the body center (heart, B1 and B2) and extracted horizontal head movements during swimming (C1 and C2).

(D and E) Sequence ranked mean swim speed (±SD; D) and velocity of the inner side of the head turn on the left (solid lines) and right (dotted lines) side (E).

(F) Distribution of the Delta curvature (left - right inner ear curvature) obtained from all swimming sequences; **** $p < 0.0001$ (Kolmogorov-Smirnov test).

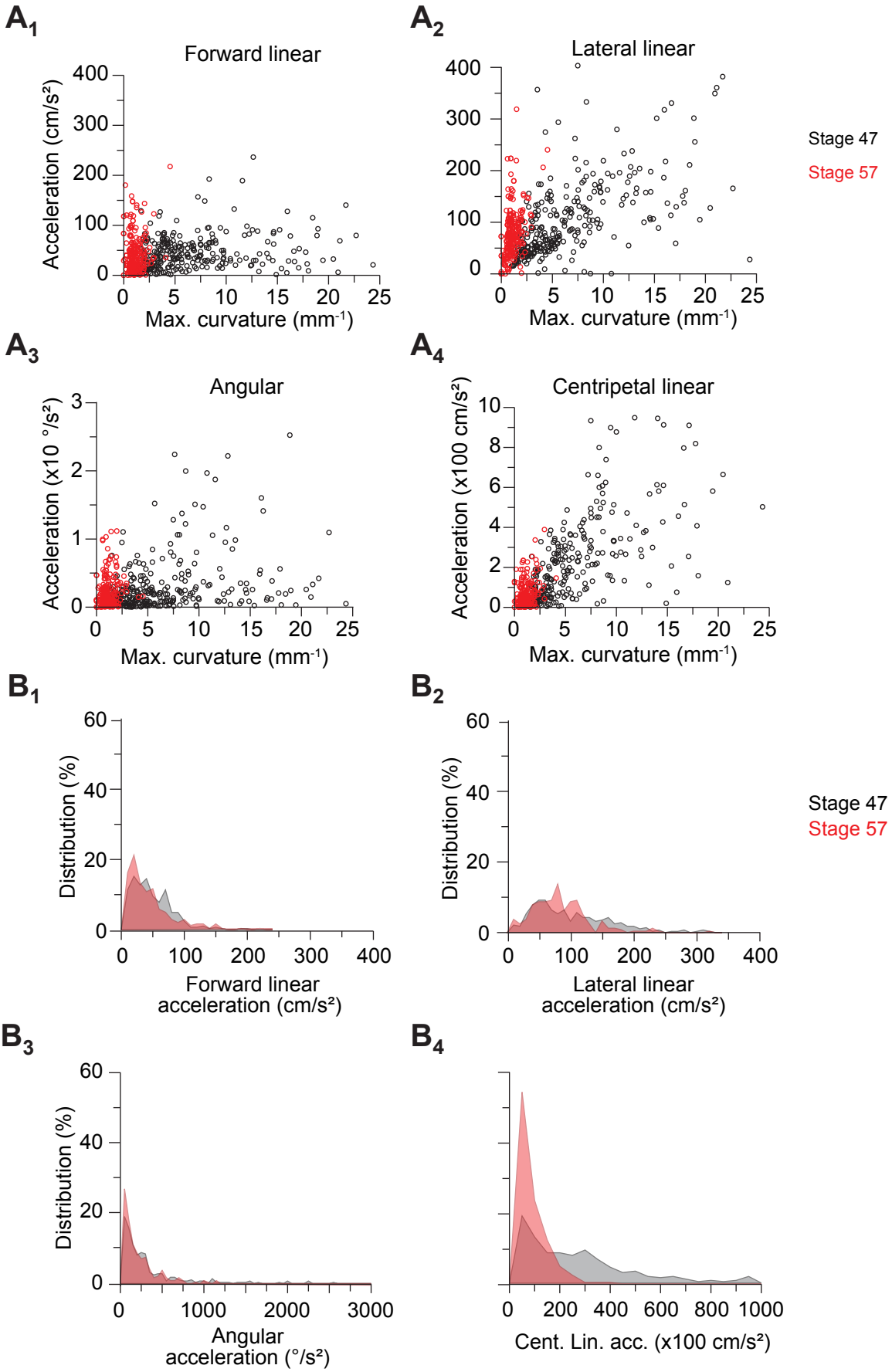
A1
Forward linear
Acceleration (cm/s²)
Max. curvature (mm⁻¹)
A2
Lateral linear
Max. curvature (mm⁻¹)
Stage 47
Stage 57
A3
Angular
Acceleration (x10 °/s²)
Max. curvature (mm⁻¹)
A4
Centripetal linear
Acceleration (x100 cm/s²)
Max. curvature (mm⁻¹)
B1
Distribution (%)
Forward linear acceleration (cm/s²)
B2
Lateral linear acceleration (cm/s²)
Stage 47
Stage 57
B3
Angular acceleration (°/s²)
B4
Cent. Lin. acc. (x100 cm/s²)

Figure S3. Magnitudes and distribution of head acceleration components during swimming. Related to Figure 2.

(A and B) Scatter plots (A) and relative distributions (B) of forward linear (A1 and B1), lateral linear (A2 and B2), angular (A3 and B3) and centripetal linear (A4 and B4) acceleration components, calculated for the OC at the peak curvature of each swimming cycle; note the marked difference in the distribution profile of centripetal linear acceleration components of stage 47 and 57 tadpoles.

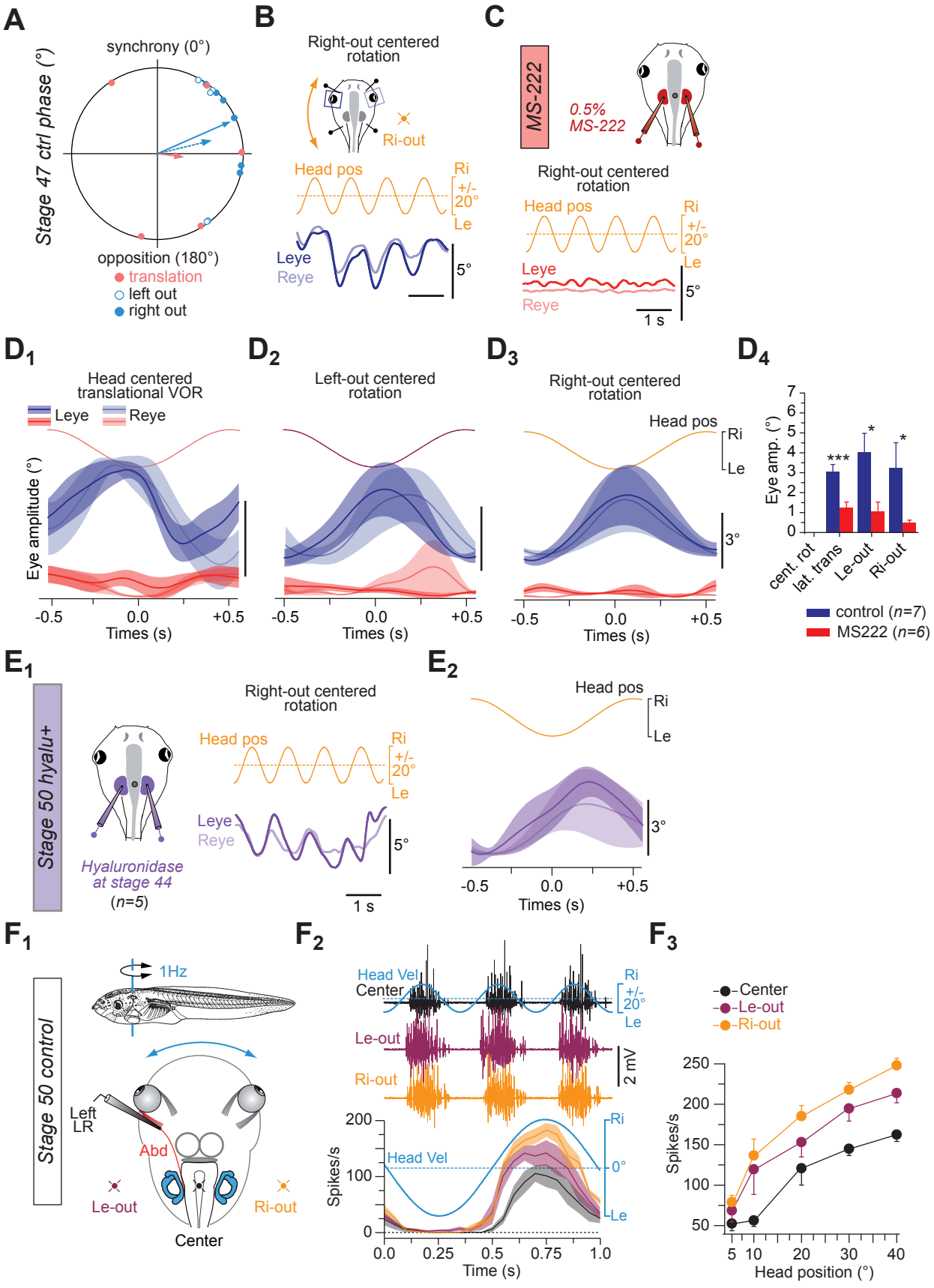
A
Stage 47 ctrl phase (°)
synchrony (0°)
opposition (180°)
translation
left out
right out
B
Right-out centered rotation
Ri-out
Head pos
Ri
+/- 20°
Le
Leye
Reye
5°
C
MS-222
0.5% MS-222
Right-out centered rotation
Head pos
Leye
Reye
1 s
D1
Head centered translational VOR
Leye
Reye
Eye amplitude (°)
Times (s)
D2
Left-out centered rotation
D3
Right-out centered rotation
Head pos
3°
D4
Eye amp. (°)
cent. rot
lat. trans
Le-out
Ri-out
control (n=7)
MS222 (n=6)
E1
Stage 50 hyalu+
Hyaluronidase at stage 44
(n=5)
Right-out centered rotation
E2
Head pos
F1
Stage 50 control
1Hz
Left LR
Abd
Le-out
Ri-out
Center
F2
Head Vel
Center
Le-out
Ri-out
2 mV
Spikes/s
Time (s)
F3
Center
Le-out
Ri-out
Spikes/s
Head position (°)

Figure S4. Eye movements and extraocular motor discharge under control conditions and after impairment of the sensory transduction. Related to Figure 3.

(A) Phase relation of cyclic eye movements during translation and rotational motion around off-center axes positioned on the left (le-out) and right side (ri-out) at stage 47 under control condition.

(B, C and D) Movement of the left (dark traces) and right (light traces) eye at stage 47 during horizontal rotation with the vertical axis off-center (Ri-out, orange) under control condition (B) and after injection of 0.5% MS-222 into both inner ears (C); note that eye movements were completely abolished by the local anesthetic. See supplemental videos 3A2 and A3.

(D) Average over a single cycle (mean ±SEM) of the left and right eye during translational motion (D1) and horizontal rotation with the position of the off-center vertical axis left-out (D2) or right-out (D3) before (blue traces) and after injection of 0.5% MS-222 (n = 6) into both inner ears on stage 47 tadpoles; note the significant reduction of the respective eye motion amplitudes after the injection (D4); * $p < 0.05$, *** $p < 0.001$ (Mann-Whitney *U*-test);

(E) Four successive motion cycles (E1) and average over a single cycle (mean ±SEM, E2) of the left and right eyes during horizontal rotation with the vertical axis off-center (Ri-out) in semicircular canal-deficient stage 50 tadpoles (n = 5); note the persistence of eye movements.

(F) Schematic of a semi-intact stage 50 whole-head preparation of larval *Xenopus* (F1) depicting abducens motor nerve recordings during horizontal rotation around a vertical axis in the center (black) or off-center on the left (Le-out, purple) or right side (Ri-out, orange); single sweeps of abducens nerve discharge during sinusoidal horizontal rotation (blue trace) around the le-out axis (top, purple), center (middle, black), and ri-out axis (bottom, orange) at 1 Hz and ±120°/s peak velocity (top traces in F2); average abducens nerve firing rate modulation (±SEM, shaded areas, bottom traces in F2) over a single motion cycle (blue trace) and firing rate (mean ±SEM) as function of peak head velocity (F3) during 1 Hz rotation around the three different axes; note that the LR nerve spike discharge, phase-timed with contraversive head peak velocity, was modulated during rotations (1 Hz; ±30 - 240°/s) around on- and off-center axes; however, peak firing rates were consistently larger for rotations around an eccentric compared to the centered axis with larger responses following rotations around the eccentric axis contralateral to the recorded LR nerve.

Video S1

Video S2

Click here to access/download

Supplemental Videos and Spreadsheets

Video S2.mp4

Click here to access/download

Supplemental Videos and Spreadsheets

Video S3.mp4

Video S4

Click here to access/download

Supplemental Videos and Spreadsheets

Video S4.mp4